Environmental Modelling and Software 188 (2025) 106395

Contents lists available at ScienceDirect

Environmental Modelling and Software

journal homepage: www.elsevier.com/locate/envsoft

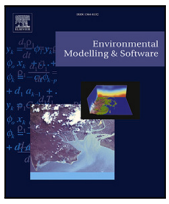

PlotToSat: A tool for generating time-series signatures from Sentinel-1 and Sentinel-2 at field-based plots for machine learning applications

Milto Miltiadou [a,b,*], Stuart Grieve [c], Paloma Ruiz-Benito [d], Julen Astigarraga [d], Verónica Cruz-Alonso [d,e], Julián Tijerín Triviño [d], Emily R. Lines [a]

[a] Department of Geography, University of Cambridge, Downing Site, Cambridge CB2 3EN, United Kingdom
[b] Department of Computer Science, University of Exeter, Innovation Centre, Exeter, EX4 4RN, United Kingdom
[c] School of Geography, Queen Mary University of London, Mile End Rd, Bethnal Green, London, E1 4NS, United Kingdom
[d] Universidad de Alcalá, Department of Life Sciences, Forest Ecology and Restoration Group (FORECO), Alcalá de Henares, Spain
[e] Universidad Complutense de Madrid, Department of Biodiversity, Ecology and Evolution, Madrid, Spain

ARTICLE INFO

Dataset link: https://github.com/Art-n-MathS/PlotToSat

Keywords:
Time-series
Forest ecology
Sentinel-1
Sentinel-2
Scalability
Plots networks

ABSTRACT

PlotToSat offers a practical and time efficient way to the challenge of extracting time-series from multiple Earth Observation (EO) datasets at numerous plots spread across a landscape. This opens up new opportunities to understand and model various ecosystems. Regarding forest ecology, plot networks play a vital role in monitoring and understanding the dynamics of forest ecosystems. These networks often contain thousands of plots arranged systematically to represent an ecosystem. Combining field data collected at plots with EO time-series will allow us to better understand phenology and ecosystem composition, structure and distribution. Linking plot networks with EO data without PlotToSat is time consuming and computational expensive because plots are small and spread out, requiring data from multiple satellite tiles. PlotToSat processed a full year of multi-tile Sentinel-1 and Sentinel-2 data (estimated 18.3TB) at 15,962 plots from the fourth Spanish Forest Inventory in less than 24 h. PlotToSat, implemented using the Python API of Google Earth Engine, offers a new and unique workflow that is innovative due to its efficient, scalable and adaptable implementation. It supports Sentinel-1 and Sentinel-2 data, but its flexible design eases integration of additional EO datasets. New environmental modelling is expected to emerge facilitating EO time-series analyses and investigating interactive effects of environmental drivers.

1. Introduction

A forest plot network contains many plots that are predetermined areas of land, systematically placed across landscapes to represent a forest ecosystem. Circular sample plots (often <1 ha) are commonly used in forest inventory because they are straightforward to establish (Packalen et al., 2023). Additionally, circles have the smallest circumference-to-area ratio, minimising the number of uncertain border trees (de Vries, 1986). A National Forest Inventory (NFI) is a plot network that consists of many sample plots, systematically chosen to be representative of the forested areas within a country. These plots spread out across a country and are revisited periodically to measure forest variables, such as tree species and diameter at breast height (DBH) (Ruiz-Benito et al., 2020), Tomppo et al. (2010). Plot networks enable ecologists to track changes over time and study various aspects of biodiversity, ecosystem structure, and ecological processes spatially. Large plot networks play a significant role in comprehending the services and functions of forest ecosystems, including species distributions (Hanewinkel et al., 2013), wood productivity (Malhi et al., 2004) and biodiversity gains and losses (Paillet et al., 2010). For instance, Hanewinkel et al. (2013) used a plot network from the International Co-operative Programme on Assessment and Monitoring of Air Pollution Effects on Forests (ICP Forests), encompassing 139 tree species from 6129 forest plots distributed regularly across Europe, and predicted suitable areas for the growth of major tree species under three climate scenarios. Plot networks provide very detailed information used for environmental modelling (Wimmler et al., 2024), but revisiting is very time-consuming and costly, severely limiting their spatio-temporal coverage due to the high expense of repeat surveys. They are, therefore, not easily scalable (i.e., it is difficult to increase spatial density and/or frequency of revisions) (Becker et al., 2023).

Forest variable collected or computed (such us tree heights and biomass) at plot regions can be used as labels to train machine learning models, but Earth Observation (EO) data can also complement the

* Corresponding author at: Department of Computer Science, University of Exeter, Innovation Centre, Exeter, EX4 4RN, United Kingdom.
E-mail address: m.miltiadou@exeter.ac.uk (M. Miltiadou).

https://doi.org/10.1016/j.envsoft.2025.106395
Received 2 August 2024; Received in revised form 28 November 2024; Accepted 20 February 2025
Available online 1 March 2025

information contained within plot networks. Plot networks often contain information about tree species, the number of trees per plot, and metrics like biomass that can be estimated for each plot region within a network. In machine learning, this information, associated with plot networks, could serve as the labels for EO data. The first application of PlotToSat for tree genera classification uses tree genera information from the fourth Spanish Forest Inventory as labels to train a k-Nearest Neighbour classifier (Miltiadou et al., 2024). Researchers can then investigate which algorithms are most effective for estimating forest variables, such as biomass and tree species using EO data. Nevertheless, through years of studies, we have managed to create descriptive indexes about vegetation and understand what information each part of the spectrum can provide about Earth. In the optical domain, the red band is sensitive to chlorophyll absorption, and changes in this band can indicate variations in chlorophyll content, while the near infra-red (NIR) band is highly reflective in healthy vegetation due to the strong scattering of NIR light by plant cell structures (Gao, 1996). For that reason, these bands are used for estimating the Normalized Difference Vegetation Index (NDVI), which is commonly used for evaluating vegetation health (Rouse et al., 1974). Additionally, the Normalised Difference Water index (NDWI) complements NDVI by capturing variations in the moisture levels of vegetation canopies (Gao, 1996). Synthetic Aperture Radar (SAR) can provide information about vertical structure and moisture content (Woodhouse, 2017) making SAR data important for estimating forest biomass (Huang et al., 2018) and detecting changes in forest cover that could indicate deforestation (Almeida-Filho et al., 2007), stress, health issues or pest attacks (Miltiadou et al., 2022). Taking into account the knowledge acquired through research about EO data, EO data can also complement the detailed information collected at forest plot networks . Plot networks and EO data can be used used combined to better understand spatio-temporal patterns in forests and their responses to climate change.

Observing plant phenology (e.g., timing of flowering and leafing) is crucial for understanding interactions between climate and ecosystems (Piao et al., 2019). To enhance our understanding of phenology, we can fuse high temporal resolution EO data for time-series analysis with plot networks. The release of the Copernicus Sentinel missions conferred increased temporal and spatial resolution. For example, Landsat 8 provides images in the visible and near-infrared parts of the spectrum at a resolution of 30 m every 16 days, while the constellation of Sentinel-2 provides images of the same parts of the spectrum at a resolution of 10 m every 5 days. This has expanded opportunities for time-series studies, including leveraging time-series of SAR data for finding associations of leafing timing for evergreen *Pinus* forest (Miltiadou et al., 2022). Nevertheless, many studies Chang and Shoshany (2016), Le Maire et al. (2011), and Andronis et al. (2022) study specific regions and require images to be downloaded to a local machine. Tools for extracting Landsat time-series (Braaten, 2021), thermal time-series derived from Landsat data (Ermida et al., 2020) and Sentinel-1 interferometric time-series (Zaki et al., 2024) have emerged.

Hamonised National Forest Inventories provide timely information about forest state and dynamics (Ruiz-Benito et al., 2020), can encompass from hundreds to thousands of plots across a country. These plots are often small (<1 ha) and widely dispersed, requiring researchers to work across multiple satellite tiles to access data corresponding to only a small number of pixels. The thermal time-series tool (Ermida et al., 2020) was implemented in JavaScript using Google Earth Engine's Code Editor, which limits flexibility for batch processing. Running the tool hundreds of thousands of times for each plot in a large network is time-consuming, and GEE supports only up to 3000 pending tasks per project. The Sentinel-2 interferometric time-series tool (Zaki et al., 2024) proposed a processing pipeline using SNAP, which requires downloading images and thus demands substantial storage space. Because these approaches are time-consuming and computationally inefficient, integrating satellite data with plot data remains largely local.

In this paper, we present a new flexible tool, PlotToSat, for creating time-series of EO data spanning over at multiple plot regions using the Python API of Google Earth Engine (GEE). We designed it to be as flexible as possible, allowing it to be tailored to the user's needs, with ongoing developments aimed at increasing its usability. PlotToSat can handle plot networks containing thousands of plots spread out to many tiles. Sentinel-1 and Sentinel-2 are the first collections (i.e., organised archives containing images acquired at varying resolutions and time periods) to be incorporated into. However, its flexible design enables the addition of more collections in the future. A time-series of multi-spectral data (Sentinel-2) spanning over a year is a spectral–temporal signature capturing both the temporal and spectral dynamics of its associated plot. A spectral–temporal signature has many applications including improving forest type mapping (Pasquarella et al., 2018) and identifying pine wilt disease at an early state (Yu et al., 2022). By running PloToSat multiple times, an extended time-series can be derived for understanding longer term landscape changes (e.g., post-fire restoration after a fire event Chen et al., 2014). The data are exported into CSV files for easy interpretation in statistical software and fused with the data of the given plot network. This allows for forest related data collected at plot regions and derived metrics, such us tree heights, carbon and species, to be used as labels for training and evaluating machine learning algorithms, as well as using EO data as complementary to plot networks. PlotToSat provides a new workflow, bringing together sensors and ground data in a way that was not previously possible. It bridges the gap between forest ecology and geography due to the integration of time-series satellite data with plot information, providing detailed temporal information about forest inventory plot networks. This eases the observation of phenological changes of forests from space and, therefore, the assessment of forest responses over time.

The usability of PlotToSat extends to other disciplines and ongoing developments aim to increase its usability. The current version of PlotToSat could be useful for any study that requires linking circular regions spread over a landscape with satellite data and monitoring spatio-temporal spectral and structural changes. This can include, but is not limited to, investigating spatial and temporal parameters associated with the spread of infectious diseases (Salje et al., 2016), assessing landsliding systems (Temme et al., 2020), quantifying urban expansion (Seto and Fragkias, 2005) and monitoring displacement at archaeological sites following earthquakes (Agapiou et al., 2013). A common application of circular samples is in the application of spatial statistics to explore clustering within irregular 2 and 3 dimensional data (Kulldorff, 1997). In geomorphology and landslide analysis, circular samples are used to calculate discrete landscape properties at appropriate scales (Grieve et al., 2016a). Ongoing developments of PlotToSat are focused on enabling the import of shapefiles containing multiple polygons and incorporating additional indices and collections. This will allow PlotToSat to extract time-series from multiple polygons of any shape, broadening its usability across various applications.

2. Methodology

2.1. Introduction

PlotToSat is a system that uses the Python API of Google Earth Engine (GEE) multi-regions EO time-series extraction. Google Earth Engine (GEE) is a cloud-based platform for large-scale geospatial analysis. It provides access to numerous collections of satellite imagery. Most of these collections have been pre-processed by GEE. For example, in Sentinel-1 SAR data, thermal noise removal, radiometric calibration, and terrain correction have been performed. For Sentinel-2 optical data, Bottom-Of-Atmosphere (BOA) reflectance products are available. Furthermore, GEE harmonises coordinate systems across image collections, and images are managed in tiles in a way that mosaicking is not required. It also provides tutorials on efficiently performing cloud and shadow masking, along with built-in filtering functions. However,

these operations are applied to individual images rather than entire collection.

The source code is available for downloading at: https://github.com/Art-n-MathS/PlotToSat published under the GNU General Public License (vesion 3). There is also a YouTube video tutorial at: https://youtu.be/ItaZjmQlyhI.

2.2. Overview

PlotToSat takes as input a plot network, containing plots spread across a landscape, and generates time-series of EO data for each plot for a given year. Fig. 1 illustrates the processing pipeline. To run PlotToSat, the user provides the plot network in a CSV file format containing the centre (longitude and latitude) of the plots, their radius (PlotToSat assumes plots are circular and have the same radius within a plot network), the coordinate system of the plot data, the desired EO collections (e.g., Sentinel-1 and/or Sentinel-2), a specified study region (e.g., a polygon defining the boundaries of a country), and the year of interest. PlotToSat adds a buffer equal to the specified radius around the centre of each plot, creating a list of circular polygons, where each polygon corresponds to a plot. PlotToSat pre-processes the bands of the EO images lying within the study region and acquired during the year of interest. PlotToSat calculates the pixel-wise monthly average of each band. This results in twelve instances of each band corresponding to the twelve calendar months of the selected year. If the user chooses to, PlotToSat applies additional masks (Section 2.4.3) to remove undesired data (e.g., areas of forest loss and land surface water). For each plot and each band, PlotToSat calculates the mean and standard deviation of the pixels inside its corresponding circular polygon. This results in twelve mean values and twelve standard deviation values of each band for each plot included in the plot network. Missing data often occur due to cloud masking are represented by gaps in the CSV files. PlotToSat provides the standard deviation alongside the mean to aid uncertainty and quality testing by the user, given the likely small size of the plot regions (the radius is often $\leq$25 m for forest studies) and the limited number of pixels that lie inside them; maximum pixel resolution of Sentinel-1 SAR and Sentinel-1 optical data is 10 m, with several bands ranging between 20 m and 60 m.

The result of a time-series produced using Sentinel-2 data spanning over a year is a spectral–temporal signature for Sentinel-2, indicating how spectral information varies across time and across the visible, near-infrared, and short-wave infrared parts of the electromagnetic spectrum. The result from Sentinel-1, however, consists of four independent temporal signatures (VV and VH polarisations from both descending and ascending orbits). This is because Sentinel-1 operates solely at the C-band, which is within the microwave range of the spectrum. Differences in the satellite's movement direction and polarisation (Section 2.4.1) result in subtle distinctions among the four Sentinel-1 time-series.

2.3. Architecture

GEE users work on two levels: the client-side, which handles user interaction and visualisation, and the server-side, which manages data processing and analysis. To fully leverage the potential of GEE, communication between the client and server should be minimised. GEE server performs computations by distributing the work of the submitted requests across many computers that process data simultaneously. Coding for GEE uses techniques from functional programming, e.g., for-loops and if-statements should be avoided. Once functions are implemented for a single image and are designed to neither depend on nor modify data outside their own scope, they can be mapped to an image collection, allowing GEE to parallelise the processing.

PlotToSat workflow was designed according to GEE standards to maximise processing efficiency, facilitating large scale analyses efficiently and removing the current processing bottleneck that exists when

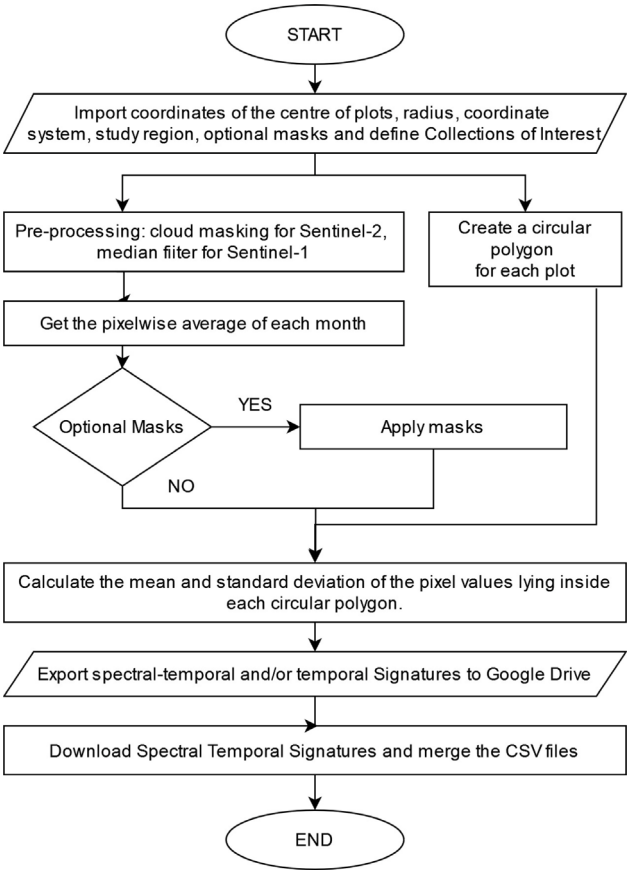

Fig. 1. The workflow of PlotToSat.

fusing plot networks with EO data. Initially, some pre-processing is done to each EO image lying within the study region and acquired during the year of interest; cloud masking is applied to Sentinel-2 multi-spectral images and speckle filtering to Sentinel-2 SAR C-band images. A function was implemented for masking out clouds from multi-spectral images and another for one filtering speckles from SAR images using a 3×3 media filter. These functions run in parallel to process many images simultaneously that exist within the study region for the specified year. The optional masks (such as the ground surface water mask) are first merged into a single combined mask, which is applied after taking the monthly pixel-wise average of each band. This process improves the efficiency of the algorithm by minimising the number of times the optional masks are applied; the results is the same as if the masks were applied to every single acquired image because the optional masks are treated as constants across different acquisition dates. However, because optional masks are treated as constants, the user needs to make adjustments in cases where masks could be variable in space or time. For example, in varying flooding extents, they may add a buffer around the ground surface water mask to ensure that all potentially affected areas are removed. It is worth noting that cropping images to the size of circular polygons and looping through them is time consuming because despite processing fewer pixels, this method is not parallelised on the cloud. This is why PlotToSat processes all the EO images in parallel first and then processes the areas within each circular polygon, also in parallel, exploiting the full capability of GEE. Furthermore, PlotToSat enforces the user to define a study region (e.g., a bounding box containing plot regions of interest) to prevent attempts to process entire collections and consequently protecting the user from GEE errors. The study regions is defined by the user using a polygon. This also allows the user to subset the plot network based

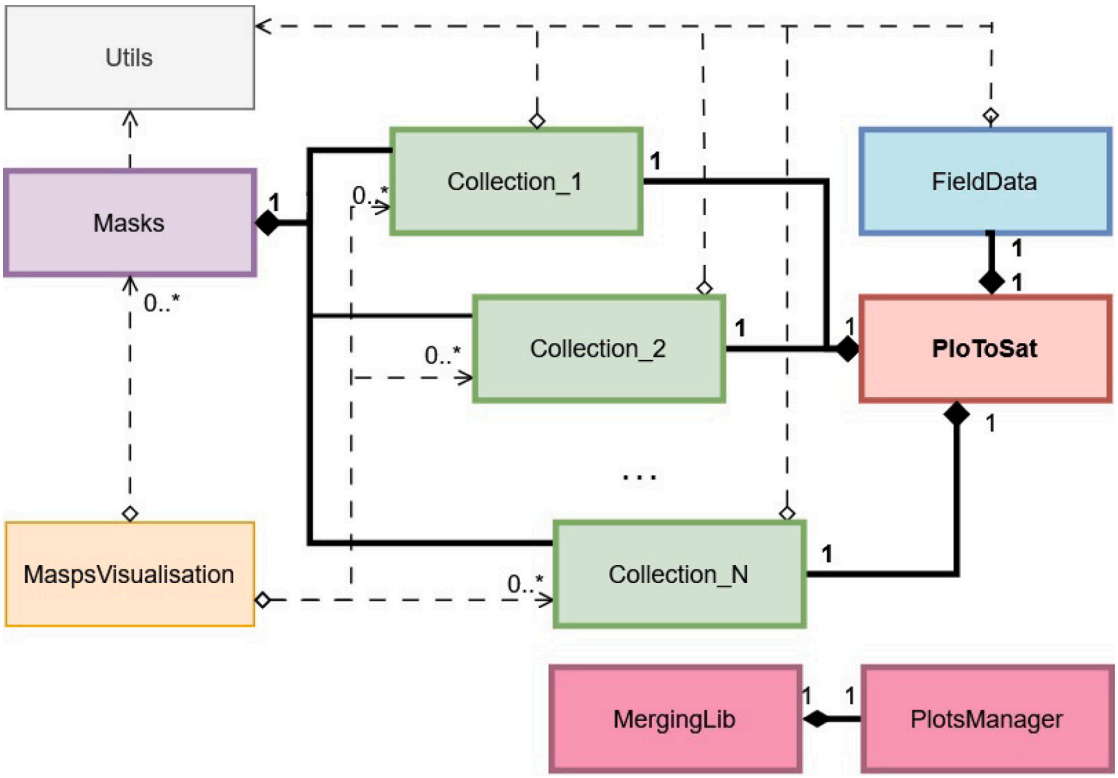

Fig. 2. Object-oriented design of the plottosat system. Each rectangle represents a module or class, with lines indicating their interactions. The PlotToSat class contains a FieldData object, one object per available collection, and uses Utils functions. Each Collection includes a Mask object and uses Utils and MapsVisualisation. User interaction is restricted to the PlotToSat class, which manages all system components and provides a simple interface. The independent MergingLib module merges the outputs of PlotToSat.

on an area of interest defined by the study region. This approach not only makes processing efficient but also contributes to reducing the energy use and, consequently, carbon footprint associated with EO data processing with PlotToSat.

Furthermore, PlotToSat demonstrates code adaptability, reusability, and flexibility, enabling straightforward code extension for the integration of new collections. This is achieved using Object-Oriented Programming (OOP), which is a modular software development approach that emulates the real world by defining reusable objects, resulting in organised code and minimising repetition (Wegner, 1990). The object-oriented design of the PlotToSat system is illustrated in Fig. 2. Users interact with the PlotToSat object, which serves as the central hub linking the system's object. Utils is a module containing a collection of stand-alone functions used across the system. Each of the other modules consists of a class, a bundle of variables and methods to perform specific tasks related to an object's purpose (e.g., FieldData class manages plot networks and all the associated interpretations are handle within that class). Each class can be used independently for other applications and it is paired with an associated test file to test and demonstrate its functionalities. The MapsVisualisation class, while external to the PlotToSat system, is used in test cases to visualise and validate outputs. The MerginLib class, also external to the core system, processes PlotToSat outputs by merging them into a single CSV file. Fig. 2 further illustrates how collection-related classes (currently implemented for Sentinel-1 and Sentinel-2) interact with the rest of the system demonstrating the simplicity of linking a new collection related class to the system. To add support for a new collection (assuming the collection is available on GEE), the user needs to create a dedicated class for that purpose and link it to the rest of the system. The rest of the system operates independently of the data type, making integration efficient.

2.4. Preprocessing steps

2.4.1. Sentinel-1

The Sentinel-1 mission is a constellation of two satellites and collects C-band SAR (Synthetic Aperture Radar) data, providing a combined revisit time of 6 days and a 10 m resolution (Fletcher, 2012). SAR systems are active sensors that operate using microwave wavelengths. They emit pulses sideways and gather information by measuring the round-trip time. The Backscatter Coefficient (σ) indicates how much radar energy is reflected back to the SAR sensor from the Earth's surface. Ascending and descending orbits denote the direction of satellite movement during SAR data acquisition. In ascending orbit, the satellite travels from south to north, whereas in descending orbit, it moves from north to south. Polarisation refers to the orientation of the electromagnetic waves emitted and received by the radar system. "V" stands for vertical orientation, "H" for horizontal, and a combination (e.g., VV, VH) indicates the transmitting orientation followed by the receiving orientation. For Sentinel-1, the backscattered coefficients σ_{VV} and σ_{VH} are obtained for ascending and descending orbits. It is worth noting that Sentinel-1 operates in dual-polarisation mode, typically using VV/VH (the polarisations used in PlotToSat). However, in certain cases, such as monitoring Arctic ice regions, it operates in HH/VV mode. The C-band (central frequency of 5.404 GHz) operates under various weather conditions, including penetrating clouds. SAR data can penetrate through objects and provide insights into the water content of trees, their dielectric constant (Ahern et al., 1993) and structural properties.

PlotToSat uses the 'COPENICUS/S1_GRD' collection from GEE. Within this collection, the data have undergone pre-processing using the Sentinel-1 Toolbox; thermal noise removal, radiometric calibration, and terrain correction have been carried out. However, SAR data contains speckle noise seen as "salt-and-pepper" artefacts (Dasari et al., 2015). To reduce the speckle noise, various filters have been

implemented. Nevertheless, filters like Mean, Frost, and Lee may blur high-variant speckle values within the data (Frost et al., 1982; Lee, 1981). Sigma and Frost filters adjust processing for improving edges within an image (Lee, 1983; Frost et al., 1982) and are, therefore, less suitable for forested areas with highly variant pixel values and no distinct edges. PlotToSat uses a 3 × 3 Median filter. The Median filter takes the median pixel value within a given window (3 × 3 in PlotToSat) effectively reducing speckles without blending noise or enhancing edges.

In mountainous regions, slopes often appear shaded due to the sideways emission of signals by SAR systems. The Fig. 3(a) displays a Sentinel-1 C band image acquired in descending orbit with polarisation VV within a mountainous expanse in Spain. Slopes facing the north-east, east, and south-east align with non-shaded areas in ascending data, while slopes facing the south-west, west, and north-west align with non-shaded areas in descending data (Miltiadou et al., 2022). After masking out data (Figs. 3(b) and 3(c)), non-shaded areas are preserved. PlotToSat offers the option to apply these masks (Section 2.4.3).

2.4.2. Sentinel-2

The Sentinel-2 mission consists of a constellation of two satellites equipped with a multi-spectral instrument, providing a 10 m resolution and a combined revisit time of 5 days (Drusch et al., 2012). PlotToSat uses harmonised Sentinel-2 L2 data from the "COPERNICUS/S2_SR_HARMONIZED" collection available on GEE. These data were processed by sen2cor (Francesco and Pignatale, 2022), providing Bottom-Of-Atmosphere reflectance data. Sentinel-2 images are often affected by clouds, necessitating their removal. PlotToSat accomplishes this in two phases:

1. Any image with a pixel cloud percentage exceeding the user-defined threshold "CLOUDY_PIXEL_PERCENTAGE" is removed.
2. Cloud and shadow masking, which involves extracting cloud masks for each image and calculating corresponding cloud shadow masks based on the sun's position (Braaten, 0000).

2.4.3. Optional masks

PlotToSat provides a range of optional masks allowing users to tailor data cleaning based on their specific scientific objectives. It currently offers five masks: (1) ground surface water mask, (2) land mask, (3) forest loss mask, (4) descending aspect mask, and (5) ascending aspect mask. Each mask is derived from a separate collection in GEE, and PlotToSat integrates them into a unified module for easy interpretation by the user. For instance, a user may choose to exclude plots near land surface water because SAR data capture both moisture and structure, resulting in signals that are not directly comparable to those of the same species in plots away from land surface water. Similarly, phenological patterns captured in the time-series can differ in disturbed areas, which, if unaccounted for, could introduce inconsistencies in downstream tasks. In other cases, users might opt to exclude plots affected by fires or other disturbances for specific years, as it may be unclear whether corresponding ground information was recorded before or after a disturbance. Excluding such areas could help reduce noise and bias in the analysis. However, the system is flexible, allowing users to decide which, if any, masks to apply based on their objectives. For example, while some may aim to exclude disturbed or near water areas to improve classification accuracy, others might retain these data to capture the broader state of the forests studied. The optional nature of these masks ensures that data preprocessing can be tailored to specific scientific needs

The ground water surface mask ('gsw') removes areas that have been heavily impacted by moisture to focus on structure information and mitigate potential noise. We use the "JRC/GSW1_0/GlobalSurfaceWater" collection (Pekel et al., 2016). Land could be masked using the Shuttle Radar Topography Mission (SRTM) digital elevation dataset ("CGIAR/SRTM90_V4") provided by Consultative Group on International Agricultural Research (CGIAR). Examples of ground surface water masking are provided in Fig. 3.

Forest loss results from factors like wildfires, urbanisation, agricultural expansion and selective logging (Curtis et al., 2018). PlotToSat can apply a forest loss mask using the Hansen Global Forest Change collection (Hansen et al., 2013), named "UMD/hansen/global_forest_change_2022_v1_10" in GEE (Fig. 3). The v10 Global Forest Change collection maps forest loss annually from 2000 to 2022. Forest loss in these maps was estimated using Landsat's red, Near-infrared (NIR) and Short-wave infrared (SWIR1 and SWIR2) spectral bands (Hansen et al., 2013). In PlotToSat, users can mask out forest loss occurring within their chosen period, from one to multiple years. This feature primarily assists researchers focusing on undisturbed areas to exclude confounding factors from their results. For instance, since fire events can alter forest ecosystems (Cochrane and Schulze, 1999), and the biomass of regenerating shrubs differs from that in unburned areas (Aranha et al., 2020), determining the rate of forest biomass gain may necessitate excluding plots in burnt areas.

An aspect map is a type of map that shows the compass direction a slope faces and by choosing the slopes aligned with the non-shaded areas of SAR data collected in ascending and descending orbit, the shaded areas in the SAR data can be removed. This is particularly important for mountainous regions (Section 2.4.1) — Fig. 3. We compute aspect maps using elevation data from the "NASA/NASADEM_HGT/001" collection, which is improved Shuttle Radar Topography Mission (SRTM) data by integrating additional information primarily from Advanced Spaceborne Thermal Emission and Reflection Radiometer (ASTER), Ice Cloud and Land Elevation Satellite (ICESat), and Geoscience Laser Altimeter System (GLAS) (Buckley et al., 2022). The slopes from 22.5° to 157.5° align with non-shaded areas in the ascending data. Similarly, the slopes from 202.5° to 337.5° align with non-shaded areas in the descending data (Miltiadou et al., 2022). Users have the option to apply both aspect maps to their corresponding ascending and descending Sentinel-1 data exclusively to retain non-shaded areas in mountainous regions. Alternatively, users can choose to apply either the ascending or descending mask to all selected collections. It is advisable not to attempt applying both ascending and descending masks simultaneously to all selected collections, as they have no overlap, meaning no pixels will be retained after masking.

3. Test case

3.1. Study area and materials

To showcase PlotToSat's utility, we tested extracting satellite information from a subset of the fourth Spanish National Forest Inventory (Spanish NFI). The fourth Spanish NFI used contained 17,300 permanent plots, of which 15,917 were within the study area (Peninsular Spain). Plots outside the study area were part of non-Peninsular Spain (e.g., the Canary Islands). Of the 15,917 plots, 15,823 belonged to the three dominant forest types, while the rest were either mixed forests, unlabelled, or needle-leaved deciduous forests. Plots have been surveyed three times since the 1980s (Fig. 4). In Spain, NFI data are collected approximately every 10 years. Plots are spaced in a 1 × 1 km UTM grid, and the collection is organised using concentric circular plots: progressively smaller circular plots are employed around a central point, with each plot surveying trees within a specific diameter at breast height (DBH) range. More information about the Spanish NFI is available at Alberdi et al. (2017). The plots were classified into four forest types: broad-leaved deciduous, broad-leaved evergreen, needle-leaved deciduous and needle-leaved evergreen (Olson et al., 2001). A forest type was assigned to a plot if 50% of basal species belonged to it Tijerín et al. (2022). Three forest types are predominantly used in this paper, (because we only had eight samples of the needle-leave deciduous forest type). Table 1 outlines the three dominant forest types,

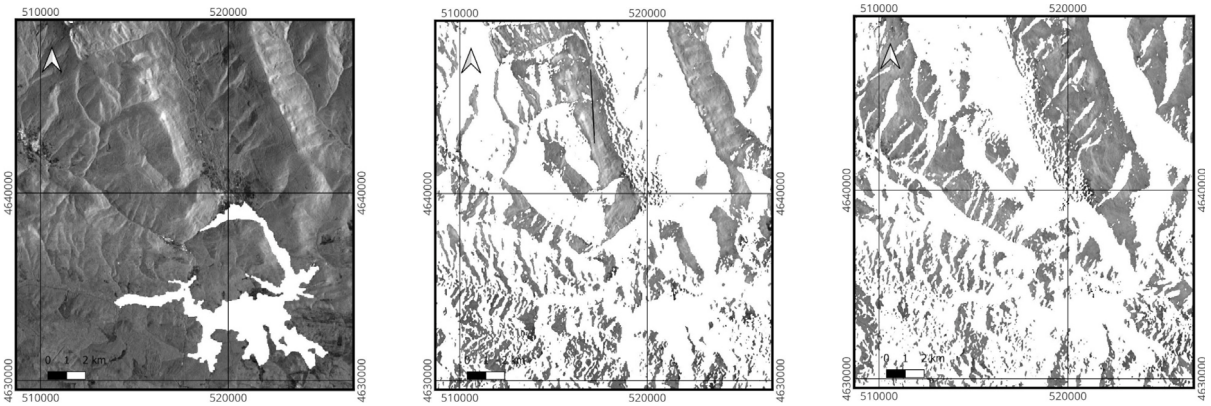

(a) Averaged 2019 descending VV Sentinel-1 data. Ground Surface Water with a 50 m buffer removed.

(b) Selected Aspects aligned with bright sides of the descending data: 202.5°–337.5°

(c) Selected Aspects aligned with bright sides of the ascending data: 2.5°–157.5°

(d) RGB image from averaged 2019 Sentinel-2 data

(e) Masking out Surface Water Mask applied with no buffer.

(f) Masking out Ground Surface Water with a 50 m buffer.

(g) Masking out Forest Loss occurred between 2000-2011.

(h) Masking out Forest Loss occurred between 2000-2011 and Ground Surface Water with a 50 m buffer.

(i) Masking out Forest Loss occurred between 2000-2022 and Ground Surface Water with a 50 m buffer.

Fig. 3. A representative selection of applying the optionally masks at a mountainous expanse by Embalse de la Cuerda del Pozo in Spain. Coordinate system EPSG:3042.

Table 1
Dominant forest types lying in the subset of the Spanish Forest Inventory used in this study, their dominant species and number of plots available per forest type.

Forest type	No of plots	Dominant species
Broad-leaved deciduous forests	3955	Quercus pyrenaica, Fagus sylvatica, Quercus robur, Quercus faginea
Broad-leaved evergreen forests	3260	Quercus ilex, Quercus suber, Eucalyptus globulus, Eucalyptus camaldulensis
Needle-leaved evergreen forests	8608	Pinus sylvestris, Pinus pinaster, Pinus halepensis, Pinus nigra

Table 2
The processing time for PlotToSat requests submitted to GEE was measured. Each row represents a set of requests for processing 300 plots from the Spanish Forest Inventory with a 25 m, 50 m or 100 m plot radius. The table shows 58 requests per radius size totalling 17,310 plots. Of these, 1392 were either outside the polygon defining the study area, Peninsular Spain, and returned an empty file or no classification was provided.

Radius size	Type of data	No of processes	No of plots per process	Mean execution time (min)	Std execution time (min)	No of failed requests
25 m	Std of Sentinel-2	58	300	23.414	9.838	0
25 m	Mean of Sentinel-2	58	300	20.643	7.661	2
25 m	Std of Sentinel-1	58	300	3.893	2.281	2
25 m	Mean of Sentinel-1	58	300	4.948	1.907	0
50 m	Std of Sentinel-2	58	300	20.293	7.786	0
50 m	Mean of Sentinel-2	58	300	20.793	7.728	0
50 m	Std of Sentinel-1	58	300	5.431	3.658	0
50 m	Mean of Sentinel-1	58	300	6.793	4.076	0
100 m	Std of Sentinel-2	58	300	19.914	7.983	0
100 m	Mean of Sentinel-2	58	300	21.759	9.215	0
100 m	Std of Sentinel-1	58	300	4.948	3.042	0
100 m	Mean of Sentinel-1	58	300	6.914	4.684	0

number of plots, and their dominant species. Plot data from the non-dominant forest type, mixed forests, unlabelled plots and plots outside the study area were included in testing execution time but excluded from other tests. Sentinel-1 and Sentinel-2 data used for testing were acquired from 2018 to 2020, with 2019 being the only year when plots were surveyed during their operation.

3.2. Testing methodology

We attempted to extract spectral–temporal and temporal signatures from Sentinel-2 and Sentinel-1 data at the 17,300 plots from the Spanish Forest Inventory (Section 3.1), but time-series for only 15,917 plots were exported as the rest lay outside the study region. We assessed PlotToSat's time performance with this large dataset. To overcome GEE's limitations in processing large amounts of data simultaneously, PlotToSat subsets the plots and generates multiple requests–one per subset–which are sent to GEE. A script is provided for merging the outputs of the multiple requests. In our test case, we processed 300 plots per request; this number is user-defined. GEE provides execution time per request. We measured the mean and standard deviation time for processing these requests, alongside the total estimated sequential execution time for comparison. This is an estimation because requests are executed in parallel, which typically results in faster processing compared to sequential execution. We also tested the execution time using three different radius sizes: 25 m (Spanish NFI size), 50 m, and 100 m (Section 3.4).

We calculated the average NDVI for each month within each forest type from the years 2018, 2019, and 2020, resulting in a time-series of twelve instances (Section 3.5). The spectral–temporal signatures from Sentinel-2, and temporal signatures from Sentinel-1 were generated for the three dominant forest types (broad-leaved deciduous, broad-leaved evergreen and needle-leaved evergreen) – Section 3.6. Sentinel-2 NDVI time-series revealed that the values observed in July provided a good distinction between the dominant forest types due to the well-separated means and reduced overlap within the standard deviation (Fig. 5). Hence, using the NDVI from July 2019 for each plot we generated histograms to analyse intra-plot variation in NDVI within dominant forest types and across different plot radius sizes (Section 3.7). Finally, for the needle-leaved evergreen forest plots, we compared the mean temporal signatures, mean spectral–temporal signatures, and the NDVI histograms using three different radius sizes: 25 m, 50 m, and 100 m (Section 3.8). The needle-leaved evergreen forest plots of July 2019 were selected because their histograms formed two peaks instead of one making it easier to visually identify variations in their distribution with varying radius sizes (Fig. 8).

3.3. Results and discussion

3.4. PlotToSat's time performance

Table 2 displays the processing time for PlotToSat requests submitted to extract the 2019 Sentinel-1 and Sentinel-2 signatures at the plots of the fourth Spanish Forest Inventory. PlotToSat allows the user to specify the size of the plot radius, while ongoing developments allow the interpretation of any set of polygons defined within a Shapefile. In the test cases presented in Table 2, we used different radius size (25 m, 50 m and 100 m). Plot size will vary depending on the user need, for example to align with ground plot size, which in forestry applications can typically vary from 0.1–10 ha. We believe that the most meaningful signatures extracted are at 25 m that corresponds to the actual radius size of the plots that we use as examples here. The 25 m radius though could contain accumulated values from nearby pixels because the maximum resolution of Sentinel 1 and 2 is 10 m, while some bands reach 60 m. It is, therefore, considered useful for the users to investigate the variations of nearby areas using bigger radius sizes (Grieve et al., 2016b). The results show that if executed sequentially, processing times would be 51.15 h, 51.53 h, and 51.75 h for 25 m, 50 m, and 100 m radii, respectively. However, parallel execution reduced processing time by more than half, resulting in finishing each radius test within less than 24 h.

As an indication of the amount of data processed for Peninsular Spain, ASF Data Search of University of Alaska offers for download approximately 2700 high-resolution Sentinel-1 image tiles acquired for one year (in 2019 VV+VH Ground Range Detected–GRD, either ascending or descending), totalling approximately 2.5 TB. Regarding Sentinel-2 Level-2 A data, according to Copernicus Open Access hub, there are around 19,500 image tiles acquired during 2019 with size ranging from 40 MB to 1200 MB each. By averaging the size of 20 images, we estimated that the size of downloading one year of L2 Sentinel-2 images covering the entire Peninsular Spain is 15.8 TB. It is important to note that while region and point time-series extraction tools are starting to emerge with GEE, they work with a single point or a single region at each execution. PlotToSat automates the extraction of numerous circular regions and provides functionalities that bypass GEE's data processing limitations (e.g., dividing processing to multiple request). It is worth highlighting that processing time is efficient with larger plot radii, as demonstrated in Table 2, where the mean execution time does not significantly vary as the radius increases. This should happen because PlotToSat preprocesses the entire collection in the study area before focusing on plot areas and because GEE uses a pyramid (multi-scale) representation of data to enable efficient processing.

At a 25 m plot radius, 2 out of the 58 automatically generated requests failed. Requests can fail for multiple reasons, such as exceeding

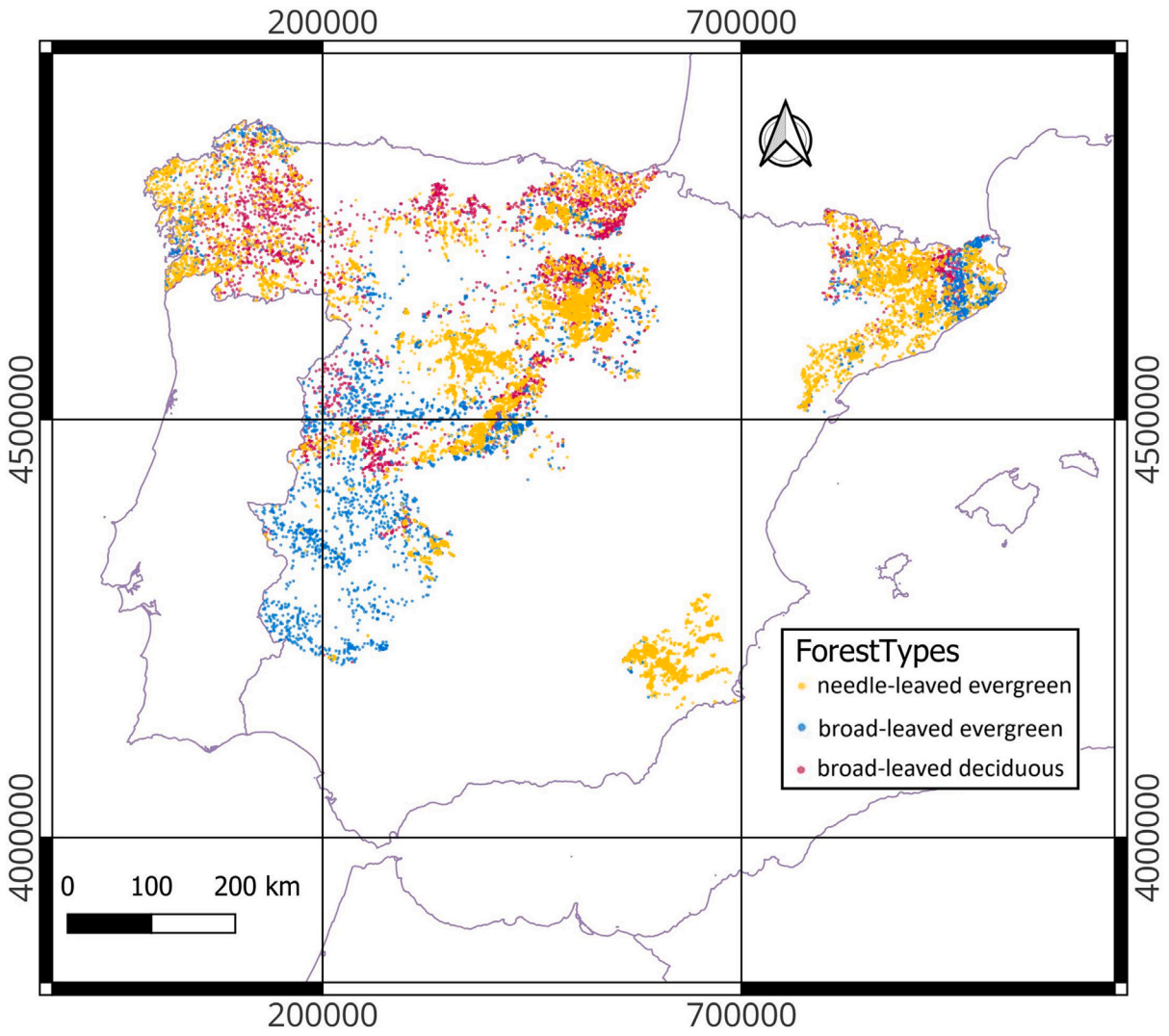

Fig. 4. Locations of the 15,823 plots representing the dominant forest types in Peninsular Spain. Coordinate system EPSG:3042.

the maximum asset storage space of 250 GB, taking too long to process, or Google Drive being full. If requests fail due to exceeding allowance in cloud storage space, we recommend reducing the number of plots processed in each request. Please note, however, that the queue for each project can hold up to 3000 tasks. If the number of plots is too small, requests exceeding that limit will not be processed. For other reasons for failure, PlotToSat offers functionality for reprocessing failed requests.

3.5. NDVI time-series

PlotToSat exports the annual monthly average values for each band from Sentinel-1 and Sentinel-2. Vegetation and other indices can be calculated using the exported data. The average NDVI for each month from 2018 to 2020 was computed for 15,917 plots across Peninsular Spain, resulting in a time-series of 12 instances per plot. Fig. 5 illustrates the mean and standard deviation of these time-series for the three dominant forest type, offering valuable phenological features for each forest type. Averaging the monthly values over three years provides a better representation of the annual phenological changes of each forest type, reducing the impact of weather conditions. From Fig. 5, we identified July as the month during which the dominant forest types can be better differentiated due to the reduced overlap between the standard deviation intervals and the well-distanced means.

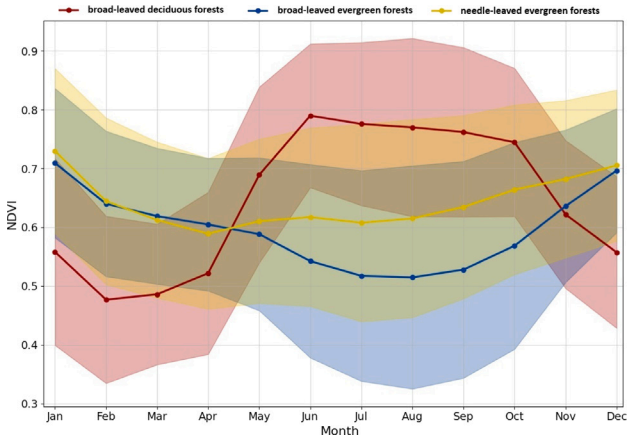

Fig. 5. The average NDVI time-series is depicted for the years 2018–2020 across the three dominant forest types. The bold solid lines show the mean and the shaded areas the standard deviation interval. We selected July as the optimal month for distinguishing the dominant forest types due to their well-separated means and reduced overlap within the standard deviation.

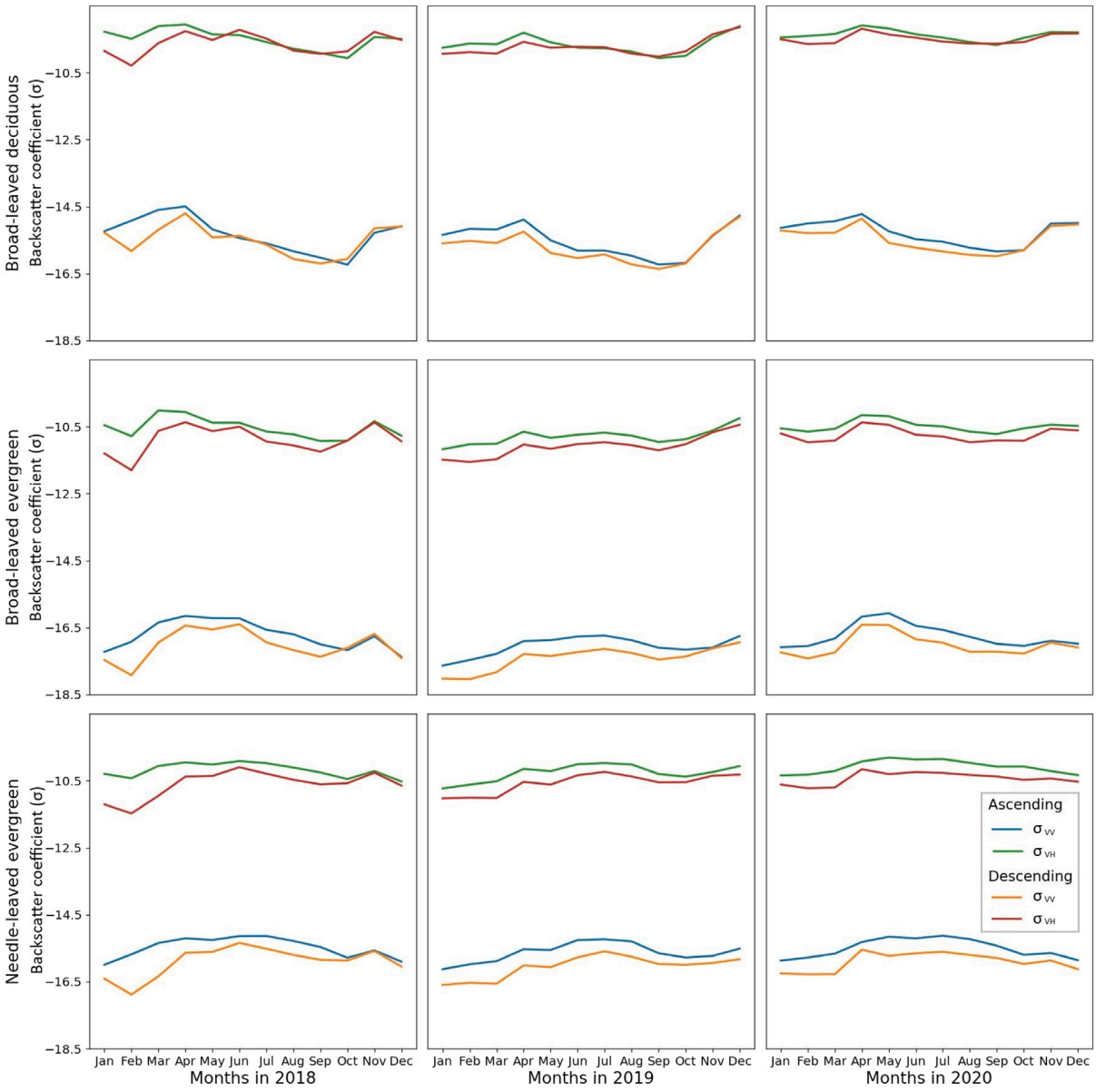

Fig. 6. The mean temporal signatures of the dominant forest types in Spain extracted from PlotToSat using plot radius 25 m and Sentinel-1 data acquired in 2018, 2019, and 2020. The backscatter coefficient (σ) measures the microwave reflectivity of the target. "Ascending" describes the satellite's path as it moves from south to north, while "descending" describes its movement from north to south. Regarding the VV and VH polarisation, 'V' stands for vertical and 'H' for horizontal, indicating the wave orientation of the emitted (first suffix) and received (second suffix) signals. They depict distinct differences between years, facilitating observation of changes potentially related to weather conditions.

3.6. Spectral temporal and temporal signatures

Figs. 6 and 7 display the mean temporal and spectral–temporal signatures, derived from Sentinel-1 and Sentinel-2 respectively, for each forest type from 2018 to 2020. The distinctiveness of each forest type's temporal and spectral–temporal signatures are illustrated, with both types of evergreen forests (broad-leaved and needle-leaved) exhibiting more similarities between them compared to broad-leaved deciduous forests. Although the signature of each forest type depicts peaks and troughs around the same time of the year, there are distinct differences between years that may arise due to varying weather conditions affecting the structure, colour, and moisture content of the forests. Associating PlotToSat's results with climate data could help in better understanding forest productivity, phenology and responses to climate change.

3.7. Histograms of NDVI values during July

Fig. 8 displays the distribution of the mean NDVI values for July from 2018 to 2020. This choice is based on the observation from Fig. 5 that NDVI during July is the month that better discriminates the three dominant forest types. The histograms in Fig. 8 does not conform to a normal distribution, particularly with evergreen forests (both needle-leaved or broad-leaved) showing two peaks. This observation aligns with Fig. 5, which illustrates that the standard deviation of NDVI in July is higher in evergreen forests. We suspect that this occurs due to the general classification of forest types, encompassing multiple subgroups of tree species. The spectral reflectances of different tree species within a forest type may form multiple subgroups (clusters). Therefore, treating them as a single subgroup (cluster) during forest type classification could result in low classification accuracy. Non-parametric methods, characterised by their flexible adaptation to the data without imposing strict distributional assumptions, may be better suited to handle the complexity of subgroups in forest type classifications.

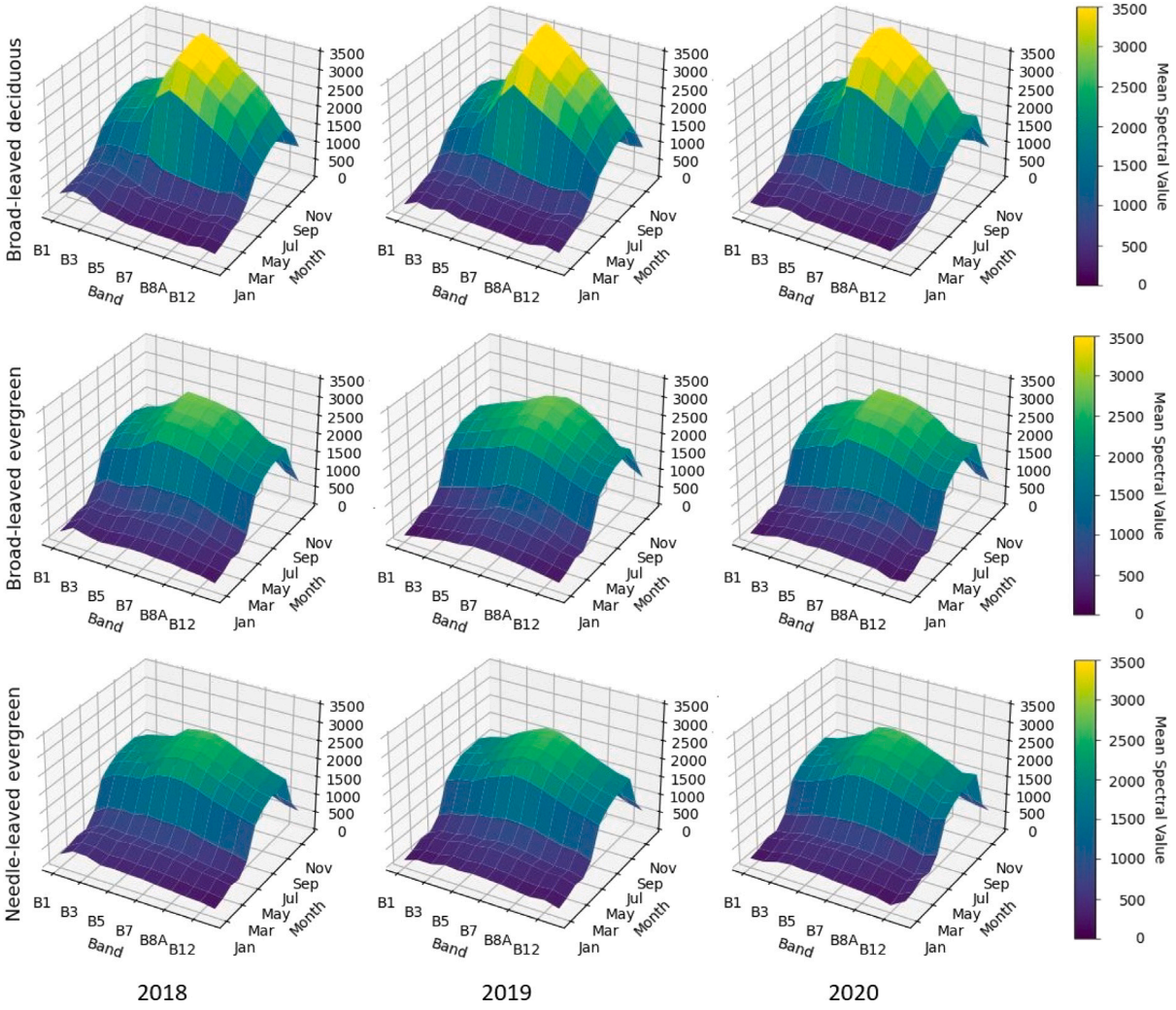

Fig. 7. The mean spectral–temporal signatures of the dominant forest types in Spain extracted from PlotToSat using Sentinel-2 data for 2018, 2019, and 2020 with 25 m plot radius (the correct Spanish Forest Inventory). They depict distinct differences between years, facilitating observation of changes potentially related to weather conditions.

3.8. Different plot radius sizes

Adjusting the radius size of plots can be a useful approach for understanding spatial landscape changes, as well as sensitivity of classification to plot size and geo-location accuracy. A smaller radius will describe the area closer to a site of interest, and wider landscape changes can be described as the distance from the site increases. With the current version, this can be investigated as an average over the radius defined from a central point, but with ongoing developments, the user will be able to adjust it. This can be useful in studies related to evaluating the extent of flooding, monitoring urbanisation, and assessing forest fire restoration in relation to its point of origin. Fig. 9 displays the mean temporal signatures from Sentinel-1 and spectral–temporal signatures from Sentinel-2 for data collected in 2019, as well as the distribution of NDVI values across with different plot radii (25 m, 50 m, and 100 m) for data acquired in July 2019. There are no distinct visual differences in the signatures with changing plot radii, indicating a high likelihood of neighbouring pixels belonging to the same forest type for most plots. Regarding the distribution of the NDVI, the distribution across different years varies more than the distribution of the same forest type across different radius sizes (Figs. 8 and 9(c)). These findings are consistent with the changes observed in temporal and spectral–temporal signatures over multiple years (Figs. 6 and 9(a) for Sentinel 1, Figs. 7 and 9(b) for Sentinel-2). Studying the annual changes in phenology and the relation with climatic conditions could help us better understand forest ecosystem responses to a changing climate.

4. Conclusions

Plot networks contain numerous plots (often circular regions) spread out systematically to adequately represent forest ecosystems. While forest ecology research depends on forest plot networks, studies for comprehending global environmental change require large spatial extents to measure forest responses (Ruiz-Benito et al., 2020). There are increasing efforts of fusing plot networks with Earth Observation (EO) data and, consequently, enriching ground-based studies. Nevertheless, plot networks spread out to multiple EO tiles, making data acquisition and processing time-consuming. Therefore, a practical way of integrating these large plot networks (often containing thousands of circular plots) with EO data creates new opportunities for understanding forest ecosystems.

In this paper, we introduced the new open-source tool PlotToSat, which streamlines the extraction of time-series EO data (one year per run) across multiple plot regions defined within a given network. PlotToSat currently supports Sentinel-1 and Sentinel-2 datasets, but its implementation is flexible and scalable; flexible because the user can select datasets of interest, as well as which masks to be applied for data cleaning and scalable because its efficient implementation can handle increasing number of plots and increasing plot radius size within

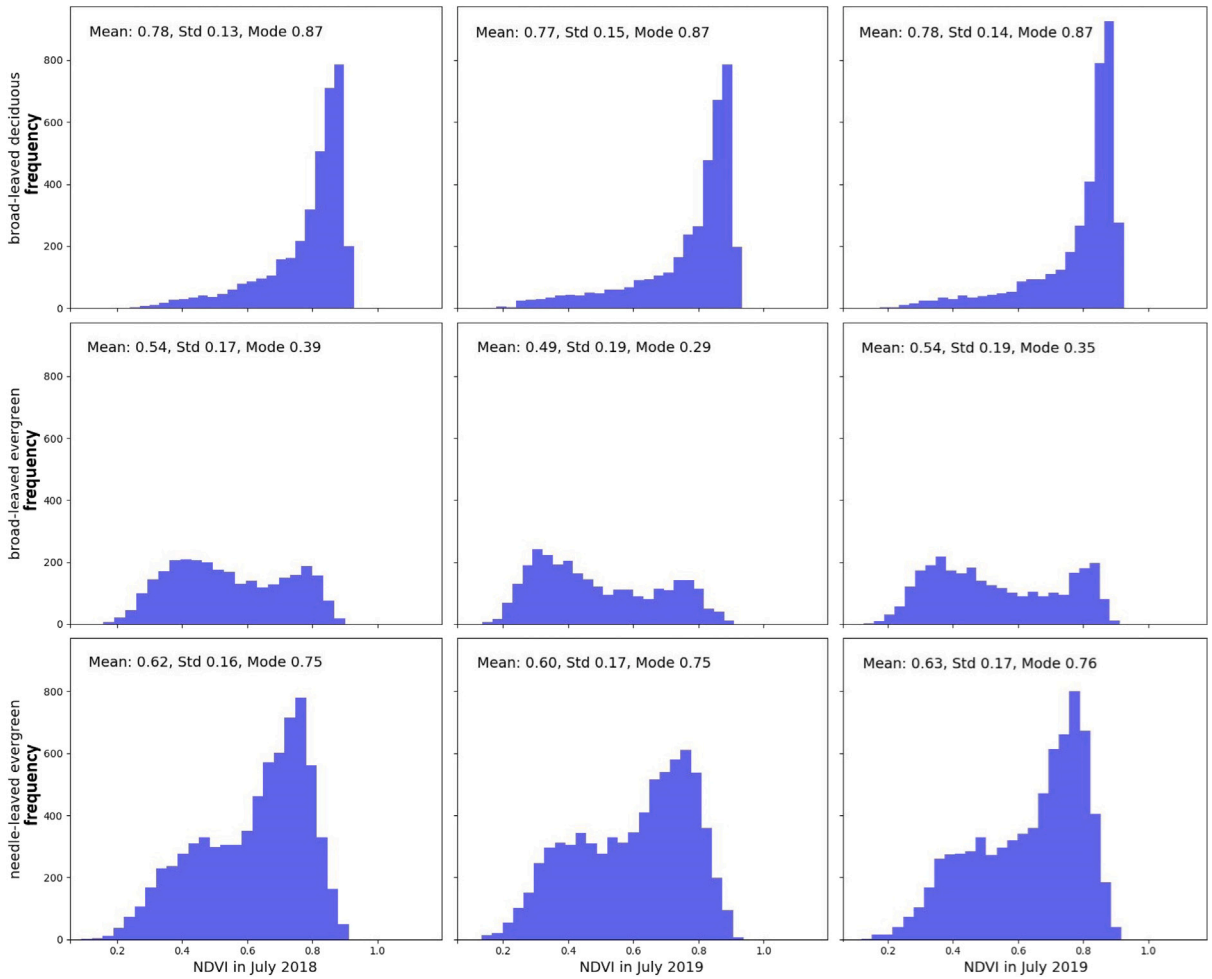

Fig. 8. The histograms of the NDVI index at each plot location for the three dominant forest types in Peninsular Spain for 2018, 2019, and 2020 with 25 m plot radius. Frequency refers to the number of occurrences of NDVI values falling within each bin. Std refers to the standard deviation and mode is the most common value within the dataset.

a plot network. Additionally, it is modular, and the main classes are independent of the dataset's type, allowing the addition of new EO datasets by predominantly implementing a new class for the collection of interest. PlotToSat extracted one year of EO time-series for 15,962 plots from the Spanish Forest Inventory (estimated 18.3TB of Sentinel-1 and Sentinel-2 data) within less than 24 h. Its efficient implementation undoubtedly outperforms downloading and processing images locally. In the future, it would be worthwhile to implement and compare similar functionalities on other platforms, such as the Copernicus Data Space Ecosystem. As far as we know, PlotToSat is the first tool that automates creations time-series for multiple large numbers of small, widely distributed regions.

A case study was conducted in Peninsular Spain. The NDVI of July was found to most clearly distinguish the dominant forest types due to the well-distanced means and reduced overlap between the standard deviation intervals. The histograms of the NDVI during July showed that they do not form a normal distribution, indicating the potential subgroups (clusters) of tree species that exist within the same forest type. The first application of PlotToSat is tree genus classification in Peninsular Spain, with results aligning with observations related to the forest type signatures used in this paper. Bias in the estimates suggests the presence of subgroups within the larger genus classes (Miltiadou et al., 2024). These subgroups may share similar properties, such as geographical region, species, stem density, or functional traits of trees. With changing radius size (25 m, 50 m, 100 m) no significant changes were observed, indicating that the sourrounding of most of the plots are likely to belong to the same forest type. Nevertheless, variations over different years were observed. It is suspected that this occurred due to varying climatic condition –e.g., Miltiadou et al. (2022) showed that warmer spring was associated with a delay in the annual SAR summer peak in *Pinus Brutia*.

On going developments will enhance the usability of PlotToSat by accommodating a wider range of applications. We aim to further support the import of shapefiles instead of a plot network, as well as the integration of nw indices and collections of data from other sensors. This will enable PlotToSat to extract time-series from a wider range of datasets at multiple regions, regardless of their shape. The exported data can be tailoired to the uses eneds, selecting bands and indices to be exported, as well as choosing between monthly averages (default) or a full time-series with values for each available image.

PlotToSat eases the extraction of time-series and, consequently, supports studies combining plot network information with EO data to better understand responses of forest ecosystems to changing climate conditions. Even though responses of various species have been studied in relation to various factors, there is still a need to better understand the interactions between multiple environmental drivers, such as temperature and precipitation combined (Ehrlén and Morris, 2015) and we have designed PlotToSat to help to enable such studies at scale. PlotToSat is not only valuable for forest ecologists but can be applied to a big range of applications from other disciplines that necessitate time-series of EO data from multiple locations spread out within a landscape.

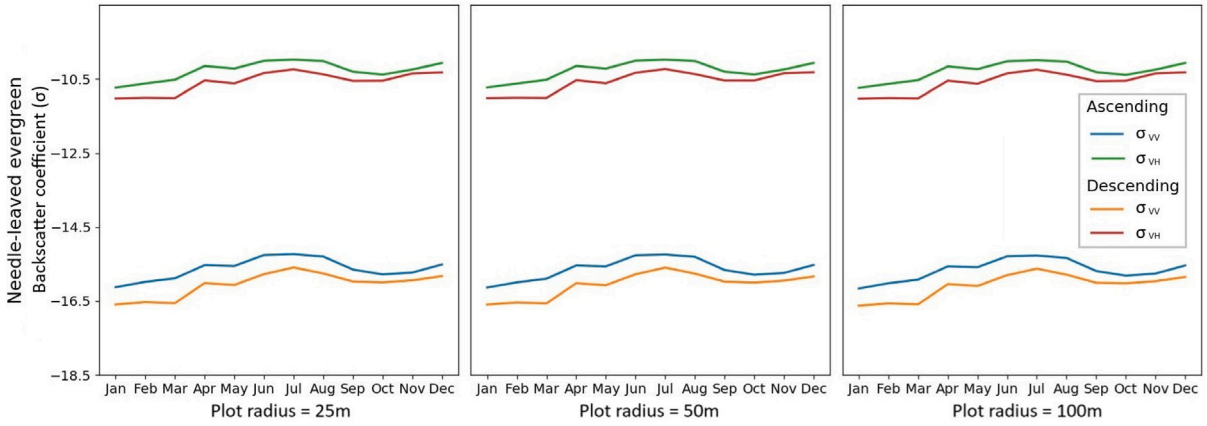

(a) Time-series of the Sentinel-1 SAR C-band backscatter coefficient

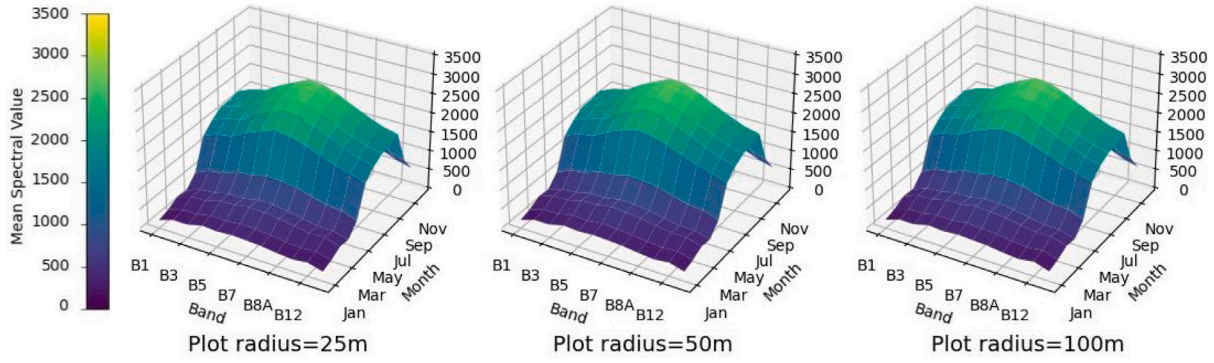

(b) Spectral-temporal signatures derived from Sentinel-2

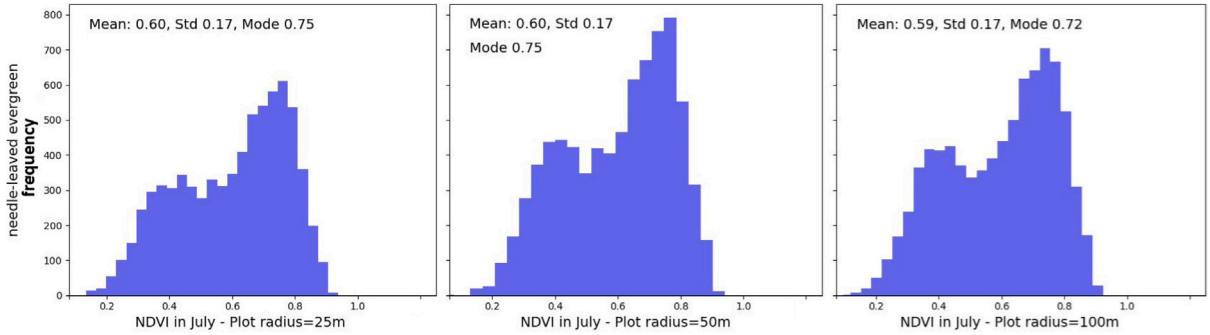

(c) Histograms of the NDVI July values

Fig. 9. 9(a) and 9(b) show temporal and spectral–temporal signatures from needle-leaved evergreen forest plots at three radius sizes: 25 m, 50 m, and 100 m. 9(c) shows histograms of the NDVI index derived using different plot radius sizes: 25 m, 50 m, and 100 m. The data used were acquired in 2019. The distribution of NDVI values forms two peaks in all cases. Minimal differences among these figures suggest forests may not significantly change over these distances.

CRediT authorship contribution statement

Milto Miltiadou: Writing – review & editing, Writing – original draft, Visualization, Validation, Software, Resources, Methodology, Investigation, Formal analysis, Data curation, Conceptualization. **Stuart Grieve:** Writing – review & editing, Supervision, Funding acquisition, Conceptualization. **Paloma Ruiz-Benito:** Writing – review & editing, Supervision, Resources, Funding acquisition, Data curation, Conceptualization. **Julen Astigarraga:** Writing – review & editing, Resources, Data curation. **Verónica Cruz-Alonso:** Writing – review & editing, Resources, Data curation. **Julián Tijerín Triviño:** Writing – review & editing, Resources, Data curation. **Emily R. Lines:** Writing – review & editing, Supervision, Project administration, Funding acquisition, Conceptualization.

Declaration of competing interest

The authors declare that they have no known competing financial interests or personal relationships that could have appeared to influence the work reported in this paper.

Acknowledgements

M. M., S. W. D. G. and E. R. L. were funded by a UKRI Future Leaders Fellowship (MR/T019832/1) awarded to E. R. L. and the University of Cambridge.

M.M. was also partially funded by the Twinning Capability for the Natural Environment (TWINE) programme, which is co- delivered by the Met Office in partnership with the Natural Environment Research Council (NERC) and is part of Earth observation investment package (EOIP)..

P. R-B. and J. A. acknowledge funding from the CLIMB-FOREST Horizon Europe Project (No 101059888) that was funded by the European Union

VCA was supported by the Ministry of Universities, Spain, and Next Generation-EU, with "Maria Zambrano" fellowship Spanish National Forest Inventory data were provided by the Spanish Ministry for the Ecological Transition and the Demographic challenge (MITECO).

Special thanks are given to Amandine Debus and Eleanor Kent, who tested PloToSat before this paper was submitted for publication.

Software and data availability

Software name: PlotToSat
Developer: Milto Miltiadou
First year available: 2024
Hardware requirements: PC/Linux
Program language: python
Software requirements: earthengine-api, ipython, pandas, and numpy
Program size: 9.3 MB (including test data and results)
Availability: https://github.com/Art-n-MathS/PlotToSat
License: GPL-3.0

Data availability

PlotToSat is openly available at https://github.com/Art-n-MathS/PlotToSat. The fourth Spanish Inventory can become available upon request to Paloma Ruiz-Benito.

References

Agapiou, A., Hadjimitsis, D.G., Sarris, A., Georgopoulos, A., Alexakis, D.D., 2013. Optimum temporal and spectral window for monitoring crop marks over archaeological remains in the Mediterranean region. J. Archaeol. Sci. 40 (3), 1479–1492. http://dx.doi.org/10.1016/j.jas.2012.10.036.

Ahern, F.J., Leckie, D.J., Drieman, J.A., 1993. Seasonal changes in relative C-band backscatter of northern forest cover types. IEEE Trans. Geosci. Remote Sens. 31 (3), 668–680.

Alberdi, I., Cañellas, I., Bombín, R.V., 2017. The Spanish National Forest Inventory: history, development, challenges and perspectives. Pesqui. Florest. Bras. 37 (91), 361–368.

Almeida-Filho, R., Rosenqvist, A., Shimabukuro, Y.E., Silva-Gomez, R., 2007. Detecting deforestation with multitemporal L-band SAR imagery: A case study in Western Brazilian Amazonia. Int. J. Remote Sens. 28 (6), 1383–1390. http://dx.doi.org/10.1080/01431160600754591.

Andronis, V., Karathanassi, V., Tsalapati, V., Kolokoussis, P., Miltiadou, M., Danezis, C., 2022. Time series analysis of landsat data for investigating the relationship between land surface temperature and forest changes in Paphos Forest, Cyprus. Remote. Sens. 14 (4), 1010.

Aranha, J., Enes, T., Calvão, A., Viana, H., 2020. Shrub biomass estimates in former burnt areas using Sentinel 2 images processing and classification. Forests 11 (5), 555.

Becker, A., Russo, S., Puliti, S., Lang, N., Schindler, K., Wegner, J.D., 2023. Country-wide retrieval of forest structure from optical and SAR satellite imagery with deep ensembles. ISPRS J. Photogramm. Remote Sens. 195, 269–286.

Braaten, J., Sentinel-2 cloud masking with s2cloudless. URL: https://developers.google.com/earth-engine/tutorials/community/sentinel-2-s2cloudless.

Braaten, J., 2021. Ee-rgb-timeseries. URL: https://github.com/jdbcode/ee-rgb-timeseries.

Buckley, S., Agram, P., Belz, J., Crippen, R., Gurrola, E., Hensley, S., Kobrick, M., Lavalle, M., Martin, J., Neumann, M., et al., 2022. Nasadem.

Chang, J., Shoshany, M., 2016. Mediterranean shrublands biomass estimation using Sentinel-1 and Sentinel-2. In: 2016 IEEE International Geoscience and Remote Sensing Symposium. IGARSS, IEEE, pp. 5300–5303.

Chen, W., Moriya, K., Sakai, T., Koyama, L., Cao, C., 2014. Monitoring of post-fire forest recovery under different restoration modes based on time series Landsat data. Eur. J. Remote. Sens. 47 (1), 153–168. http://dx.doi.org/10.5721/EuJRS20144710.

Cochrane, M.A., Schulze, M.D., 1999. Fire as a recurrent event in tropical forests of the eastern amazon: effects on forest structure, biomass, and species composition 1. Biotropica 31 (1), 2–16.

Curtis, P.G., Slay, C.M., Harris, N.L., Tyukavina, A., Hansen, M.C., 2018. Classifying drivers of global forest loss. Sci. 361 (6407), 1108–1111.

Dasari, K., Anjaneyulu, L., Jayasri, P., Prasad, A., 2015. Importance of speckle filtering in image classification of SAR data. In: 2015 International Conference on Microwave, Optical and Communication Engineering. ICMOCE, IEEE, pp. 349–352.

de Vries, P.G., 1986. Sampling with circular plots. In: Sampling Theory for Forest Inventory: A Teach-Yourself Course. Springer, pp. 212–222.

Drusch, M., Del Bello, U., Carlier, S., Colin, O., Fernandez, V., Gascon, F., Hoersch, B., Isola, C., Laberinti, P., Martimort, P., et al., 2012. Sentinel-2: ESA's optical high-resolution mission for GMES operational services. Remote Sens. Environ. 120, 25–36.

Ehrlén, J., Morris, W.F., 2015. Predicting changes in the distribution and abundance of species under environmental change. Ecol. Lett. 18 (3), 303–314.

Ermida, S.L., Soares, P., Mantas, V., Göttsche, F.-M., Trigo, I.F., 2020. Google earth engine open-source code for land surface temperature estimation from the landsat series. Remote. Sens. 12 (9), 1471. http://dx.doi.org/10.3390/rs12091471.

Fletcher, K., 2012. SENTINEL 1: ESA's Radar Observatory Mission for GMES Operational Services. European Space Agency.

Francesco, C., Pignatale, T., 2022. Sen2Cor 2.11.00 configuration and user manual. In: Copernicus Space Component Sentinel Optical Imaging Mission Performace Cluster Service.

Frost, V.S., Stiles, J.A., Shanmugan, K.S., Holtzman, J.C., 1982. A model for radar images and its application to adaptive digital filtering of multiplicative noise. IEEE Trans. Pattern Anal. Mach. Intell. (2), 157–166.

Gao, B.-C., 1996. NDWI—A normalized difference water index for remote sensing of vegetation liquid water from space. Remote Sens. Environ. 58 (3), 257–266. http://dx.doi.org/10.1016/S0034-4257(96)00067-3.

Grieve, S.W., Mudd, S.M., Hurst, M.D., 2016a. How long is a hillslope? Earth Surf. Process. Landf. 41 (8), 1039–1054. http://dx.doi.org/10.1002/esp.3884.

Grieve, S.W., Mudd, S.M., Milodowski, D.T., Clubb, F.J., Furbish, D.J., 2016b. How does grid-resolution modulate the topographic expression of geomorphic processes? Earth Surf. Dyn. 4 (3), 627–653. http://dx.doi.org/10.5194/esurf-4-627-2016.

Hanewinkel, M., Cullmann, D.A., Schelhaas, M.-J., Nabuurs, G.-J., Zimmermann, N.E., 2013. Climate change may cause severe loss in the economic value of European forest land. Nat. Clim. Chang. 3 (3), 203–207.

Hansen, M.C., Potapov, P.V., Moore, R., Hancher, M., Turubanova, S.A., Tyukavina, A., Thau, D., Stehman, S.V., Goetz, S.J., Loveland, T.R., et al., 2013. High-resolution global maps of 21st-century forest cover change. Sci. 342 (6160), 850–853.

Huang, X., Ziniti, B., Torbick, N., Ducey, M.J., 2018. Assessment of forest above ground biomass estimation using multi-temporal C-band Sentinel-1 and polarimetric L-band PALSAR-2 data. Remote. Sens. 10 (9), 1424.

Kulldorff, M., 1997. A spatial scan statistic. Comm. Statist. Theory Methods 26, http://dx.doi.org/10.1080/03610929708831995.

Le Maire, G., Marsden, C., Nouvellon, Y., Grinand, C., Hakamada, R., Stape, J.-L., Laclau, J.-P., 2011. Modis ndvi time-series allow the monitoring of Eucalyptus plantation biomass. Remote Sens. Environ. 115 (10), 2613–2625.

Lee, J.-S., 1981. Refined filtering of image noise using local statistics. Comput. Graph. Image Process. 15 (4), 380–389.

Lee, J.-S., 1983. Digital image smoothing and the sigma filter. Comput. Vis. Graph. Image Process. 24 (2), 255–269.

Malhi, Y., Baker, T.R., Phillips, O.L., Almeida, S., Alvarez, E., Arroyo, L., Chave, J., Czimczik, C.I., Fiore, A.D., Higuchi, N., et al., 2004. The above-ground coarse wood productivity of 104 Neotropical forest plots. Global Change Biol. 10 (5), 563–591.

Miltiadou, M., Karathanassi, V., Agapiou, A., Theocharidis, C., Kolokousis, P., Danezis, C., 2022. A selection of experiments for understanding the strengths of time series SAR data analysis for finding the drivers causing phenological changes in Paphos Forest, Cyprus. Remote. Sens. 14 (15), 3581. http://dx.doi.org/10.3390/rs14153581.

Miltiadou, M., Lines, E.R., Grieve, S., Benito, P.R., Astigarraga, J., Cruz, V., 2024. Tree genera classifications in Spain using time-series sentinel-2 data extracted from plottosat. In: IGARSS 2024-2024 IEEE International Geoscience and Remote Sensing Symposium. IEEE, pp. 4953–4956. http://dx.doi.org/10.1109/IGARSS53475.2024.10641135.

Olson, D.M., Dinerstein, E., Wikramanayake, E.D., Burgess, N.D., Powell, G.V., Underwood, E.C., D'amico, J.A., Itoua, I., Strand, H.E., Morrison, J.C., et al., 2001. Terrestrial ecoregions of the world: A new map of life on earth: A new global map of terrestrial ecoregions provides an innovative tool for conserving biodiversity. BioScience 51 (11), 933–938.

Packalen, P., Strunk, J., Maltamo, M., Myllymäki, M., 2023. Circular or square plots in ALS-based forest inventories—does it matter? Forestry 96 (1), 49–61. http://dx.doi.org/10.1093/forestry/cpac032.

Paillet, Y., Bergès, L., Hjältén, J., Ódor, P., Avon, C., Bernhardt-Römermann, M., Bijlsma, R.-J., De Bruyn, L., Fuhr, M., Grandin, U., et al., 2010. Biodiversity differences between managed and unmanaged forests: Meta-analysis of species richness in Europe. Conserv. Biol. 24 (1), 101–112.

Pasquarella, V.J., Holden, C.E., Woodcock, C.E., 2018. Improved mapping of forest type using spectral-temporal landsat features. Remote Sens. Environ. 210, 193–207.

Pekel, J.-F., Cottam, A., Gorelick, N., Belward, A.S., 2016. High-resolution mapping of global surface water and its long-term changes. Nat. 540 (7633), 418–422.

Piao, S., Liu, Q., Chen, A., Janssens, I.A., Fu, Y., Dai, J., Liu, L., Lian, X., Shen, M., Zhu, X., 2019. Plant phenology and global climate change: Current progresses and challenges. Global Change Biol. 25 (6), 1922–1940. http://dx.doi.org/10.1111/gcb.14619.

Rouse, J.W., Haas, R.H., Schell, J.A., Deering, D.W., et al., 1974. Monitoring vegetation systems in the great plains with ERTS. NASA Spec. Publ. 351 (1), 309.

Ruiz-Benito, P., Vacchiano, G., Lines, E.R., Reyer, C.P., Ratcliffe, S., Morin, X., Hartig, F., Mäkelä, A., Yousefpour, R., Chaves, J.E., et al., 2020. Available and missing data to model impact of climate change on European forests. Ecol. Model. 416, 108870. http://dx.doi.org/10.1016/j.ecolmodel.2019.108870.

Salje, H., Lessler, J., Paul, K.K., Azman, A.S., Rahman, M.W., Rahman, M., Cummings, D., Gurley, E.S., Cauchemez, S., 2016. How social structures, space, and behaviors shape the spread of infectious diseases using chikungunya as a case study. Proc. Natl. Acad. Sci. 113 (47), 13420–13425. http://dx.doi.org/10.1073/pnas.1611391113.

Seto, K.C., Fragkias, M., 2005. Quantifying spatiotemporal patterns of urban land-use change in four cities of China with time series landscape metrics. Landsc. Ecol. 20, 871–888. http://dx.doi.org/10.1007/s10980-005-5238-8.

Temme, A., Guzzetti, F., Samia, J., Mirus, B.B., 2020. The future of landslides' past—a framework for assessing consecutive landsliding systems. Landslides 17, 1519–1528. http://dx.doi.org/10.1007/s10346-020-01405-7.

Tijerín, T.-J., Moreno-Fernández, D., Zavala, M.A., Astigarraga, J., García, M., 2022. Identifying forest structural types along an aridity gradient in peninsular Spain: Integrating low-density LiDAR, forest inventory, and aridity index. Remote. Sens. 14 (1), 235. http://dx.doi.org/10.3390/rs14010235.

Tomppo, E., Gschwantner, T., Lawrence, M., McRoberts, R.E., Gabler, K., Schadauer, K., Vidal, C., Lanz, A., Ståhl, G., Cienciala, E., et al., 2010. National forest inventories. In: Pathways for Common Reporting. Vol. 1, European Science Foundation, pp. 541–553.

Wegner, P., 1990. Concepts and paradigms of object-oriented programming. ACM Sigplan Oops Messenger 1 (1), 7–87.

Wimmler, M.-C., Bathmann, J., Vollhüter, J., Berger, U., 2024. Pymanga: A modular, open and extendable software platform for modeling of forest and vegetation dynamics. Environ. Model. Softw. 174, 105973.

Woodhouse, I.H., 2017. Introduction to Microwave Remote Sensing. CRC Press.

Yu, R., Huo, L., Huang, H., Yuan, Y., Gao, B., Liu, Y., Yu, L., Li, H., Yang, L., Ren, L., et al., 2022. Early detection of pine wilt disease tree candidates using time-series of spectral signatures. Front. Plant Sci. 13, 1000093. http://dx.doi.org/10.3389/fpls.2022.1000093.

Zaki, A., Chang, L., Manzella, I., van der Meijde, M., Girgin, S., Tanyas, H., Fadel, I., 2024. Automated python workflow for generating sentinel-1 PSI and SBAS interferometric stacks using SNAP on geospatial computing platform. Environ. Model. Softw. 178, 106075.